Mapping of Elastic Anisotropy with Air-Coupled Phonon-Focusing of Guided and Surface Waves

I. SOLODOV, D. DÖRING and G. BUSSE, Institute for Polymer Testing and Polymer Science (IKP), Non-destructive Testing (ZFP), University of Stuttgart, Stuttgart, Germany

Abstract. Acoustic wave propagation in anisotropic media is accompanied by focusing of elastic energy along certain directions (phonon focusing). The phonon focusing has been widely used to study a variety of anisotropic material properties including thermal conductivity, phonon scattering, super-lattices, and transport of electron-hole droplets in solids. Mainly low-frequency bulk phonons were studied (bulk acoustic waves) generated by a point-like optical (laser) or contact acoustic sources. This paper reports the first observation of guided phonons (i.e. plate and surface waves) generated in a wide angular spectrum using focused air-coupled ultrasound. Such an air-coupled version of phonon focusing is advantageous for NDT applications due to non-contact probing of material properties. The results of applications demonstrate the feasibility of the method for mapping of elastic anisotropy over large areas in engineering materials (polycrystalline alloys, polymers, composites, etc.) where it manifests in meso- and macro-scale structures due to internal stresses, texture, molecular and fibre orientation.

1. Introduction

The majority of current and newly developing materials (polymers, composites, ceramics, nano-structures, etc.) exhibit an evident elastic anisotropy which provides anomalous physical properties and a wide range of applications. Mapping of elastic anisotropy is a sensitive tool for testing material structure and strength, monitoring of product quality and its degradation caused by environmental factors or deviations in manufacturing process, progression of damage, etc. A flexible and reliable engineering technology capable of providing such measurements on-line in industrial environment is not available at present.

Elastic anisotropy strongly affects acoustic wave propagation in solids: the wave velocity, energy flux and polarization depend on the propagation direction. These effects were studied in detail for bulk acoustic waves [1] but much less attention has been paid to the guided wave anisotropy in specimens of finite thickness. The energy transport by acoustic waves simulates heat transfer by high-frequency phonons, which is also determined by elastic anisotropy. This link motivated a boom of research activity on phonon focusing, i.e. observation of anisotropic energy transfer (focusing) by the phonons in frequency range from low-MHz up to near-THz [2]. The phonon focusing experiments are based on imaging of acoustic wavefronts emanating from a point-like source of phonons (acoustic waves). Numerous experiments in this field were mainly concerned with propagation of laser-generated short pulses of bulk acoustic waves [3, 4] and surface waves [5, 6] in cubic crystals. Contact [7] or water-coupled [8] acoustic excitation-detection schemes with piezo-transducers were also reported in phonon focusing experiments in the low-MHz frequency range.

In this paper, a fully non-contact hybrid air-coupled/optic configuration for phonon focusing of guided (flexural) and surface waves is developed and applied to mapping of elastic anisotropy. A theoretical background of the technique is presented and followed by experimental results obtained for composite materials. It is shown that the method can provide a rapid interrogation of material anisotropy and its uniformity over large areas.

2. Theoretical background

The scheme of the air-coupled ultrasound (ACU) based phonon focusing is shown in Figure 1. A guided/surface wave (continuous wave mode) is generated by a focused air-coupled transducer with a variable angle of incidence θ (0 – 90^0) which can provide both cylindrical (at θ=0) and plane flexural/surface wave excitation. The wave field is visualized with a laser vibrometer responding to the out-of-plane component of vibration velocity.

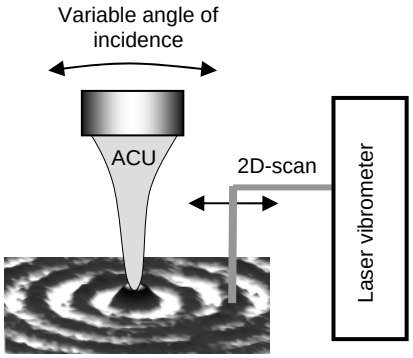

Figure 1. Layout of air-coupled phonon-focusing.

2.1 Wave Excitation with a Point-Like Air-Coupled Source

At normal incidence (θ=0), a focused beam of air-coupled ultrasound creates a localized time-varying pressure on a solid surface that can cause flexural/surface waves in, correspondingly, thin/thick plate-like specimens. A vertical polarization of both waves facilitates the air-coupled excitation. According to calculations [9], the ratio of out-of-plane/in-plane displacement components is >> 1 for flexural waves in thin plates ($k_t D < 1$, k_t is the wave number of shear wave, D is the plate thickness). By $k_t D$=30, the guided waves transform into surface waves whose polarization ratio changes in the range of ≅ (1.3 – 1.9) for all solid materials [10].

The efficiency of excitation also depends on the amplitude of acoustic pressure and the profile of an air-coupled beam at the surface. For an air-coupled ultrasound beam of intensity *J*, the pressure amplitude above the surface is found as $p_m = (2JZ)^{1/2}$, where *Z* is the acoustic impedance of air ($\approx 4 \cdot 10^{-4}$ Mrayl). Since *Z* is 3-4 orders lower than acoustic impedance in solids, the stress amplitude below the surface is $2\,p_m$. In a solid with the Young modulus *E*, it produces a local surface strain $\varepsilon = 2p_m / E$ which is a source of the wave motion with maximum displacement $u = \varepsilon / k$, where k is the wave number.

To prevent overheating and damage of piezo-composite air-coupled transducers, maximum voltage applied in the CW mode should be around 15-20V p/p. For typical

insertion losses of 20-30 dB, it results in a few mW of acoustic power (P) radiated by the surface of the transducer (S) and ultrasound intensity $J = P/S \sim 1$ mW/cm^2. The acoustic intensity in the focus area (S_f) is therefore $J(S/S_f)$ and for weakly-focused transducers (angular aperture $2\gamma_0 = (20\text{-}30)^0$) can increase up to ~ (10-20) mW/cm^2. The pressure amplitude above the surface is then estimated as ~ (300 – 400) Pa producing in a material like PMMA ($E \cong (3-4)$ GPA) the strain $\varepsilon \sim 10^{-7}$. Hence, the displacement amplitude that drives wave motion (frequency 400-kHz; velocity $v \sim 10^3$ m/s) is expected to be ~(10^{-10}-10^{-11})m which is nonetheless detectable within the operation range of commercial scanning vibrometers.

Another factor important for efficient wave excitation is concerned with the size of the focus area of the air-coupled beam. For a spherically focused field, the radius at which the beam intensity becomes zero is [11] $r_0 = 0.61\,\lambda/\sin\gamma_0$, where $\sin\gamma_0 = a/d$ (a is the radius of the transducer, d is the focus length). The wave field generated by such a cylindrically symmetrical source (~ $\exp(j\omega t)$) can be represented by the Hankel transform as a spectrum of "cylindrical harmonics":

$$u(r) = \int_0^\infty (W(k)/k) J_0(kr) k dk\,, \tag{1}$$

where $J_0(kr)$ is a Bessel function of zero-order of the first kind, and $W(k)$ is the spectrum of spatial frequencies (radial wave numbers k).

The efficiency of excitation of a cylindrical wave with a certain wavenumber k is proportional to $W(k)$ that can be found by using the inverse Hankel transform:

$$W(k) = k\int_0^\infty u(r) J_0(kr) r dr, \tag{2}$$

which for $u(r) = u_0$ $(0 \le r \le r_0)$ and $u(r) = 0$ $(r > r_0)$ takes a simple form:

$$W(k) = r_0 u_0 J_1(kr_0)\,, \tag{3}$$

where $J_1(kr_0)$ is a Bessel function of the first order of the first kind. This function oscillates strongly as kr_0 changes with successive maxima corresponding to $kr_0 \approx 3.8$; 5.2;…[12]. Thus, to optimize the excitation, the diameter of the focus spot should be chosen as $2r_0/\lambda_S \approx 0.44$; 1.65…, where λ_S is the wavelength of the waves excited in the solid. On the contrary, minima of the excitation efficiency will be observed when $J_1(kr_0) \approx 0$ that corresponds to the spot size close to multiples of the wavelength ($2r_0/\lambda_S \approx 1.2$; 2.2; …). According to the above, for a given value of λ_S the excitation efficiency is managed by a proper choice of the transducer aperture γ_0.

2.2 Wavefront Pattern and Material Anisotropy

The shape of the wavefront radiated by the point-like source displays the in-plane anisotropy of the material. For quantitative NDT applications, the wavefront pattern has to be used to derive material stiffness. This requires the analysis of the velocity data which the pattern reveals. An example given in Figure 2 shows the elliptical wavefront pattern one would expect for a unidirectional composite material. It clearly demonstrates that each section of the wavefront is transported with the energy propagation (or group) velocity ($\vec{v}_g$) at the angle (ψ) to the wave vector $\vec{k}$ [2].

The deviation of the energy velocity pattern from a circle is a qualitative indicator of elastic anisotropy. However, to quantify the in-plane material stiffness it is better to use the phase velocity which is usually a simpler function of elastic moduli. The relation between the group and phase velocities [1] is easily seen from Figure 2:

$$v_p = v_g \cos\psi \,. \tag{4}$$

The angle ψ is determined by a local curvature of the curve in Fig. 2 [12]:

$$tg\,\psi = (1/v_g)dv_g / d\varphi \,. \tag{5}$$

By combining (4) and (5) we obtain:

$$v_p = v_g[1 + (1/v_g)dv_g / d\varphi]^{-1/2} \,. \tag{6}$$

The calculations of the phase velocity pattern from the energy flow data based on relation (6) are illustrated in Figure 2 (right). In general, the difference between the curves depends on the shape of the wavefront ellipse but reduces to zero along the symmetry axes.

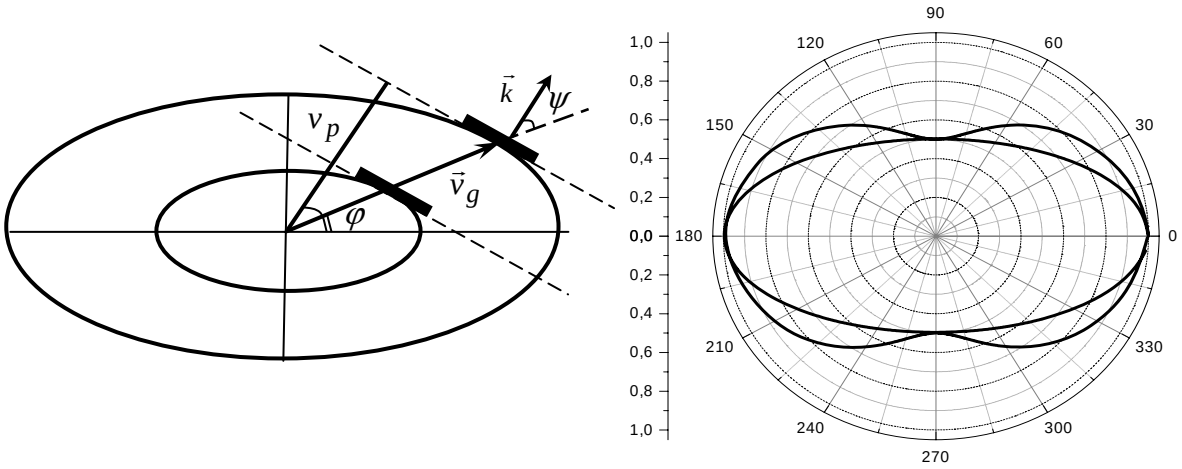

Figure 2. Energy flow and phase velocity in wavefront pattern (left); reconstruction of phase velocity pattern from elliptical wavefront (right).

3. Experimental

The experimental set-up for air-coupled phonon-focusing is shown in Figure 1. A 395-kHz CW 15V p/p voltage is applied to the weakly focused air-coupled piezo-composite transducer which launches ultrasonic waves on the top surface of the specimen. The flexural/surface wave field is scanned with a laser vibrometer responding to the out-of-plane component of the vibration velocity. To analyse the total area of the specimen at $\theta = 0$, scanning is normally made across the rear surface of the plate; alternatively, a single-sided access is used for an oblique AC-incidence. The output signal of the vibrometer is compared with the reference voltage (AC-input) to result in recording of the phase synchronised time traces of the vibration velocity for each position of the laser beam. The data acquired over the specimen surface are colour coded and played back as a time sequence of frames, thereby displaying an animated picture of wave propagation. The frames are then used for wavefront imaging and read-out of local phase, amplitude, or wavelength of the flexural/surface waves.

To estimate the acoustic power of the focused beam we measured a radiation force exerted by ultrasound on a target in air. A piece of thin aluminium foil attached to a carbon

thread (total weight 12 mg) was used in a pendulum configuration and the angle of deflection in ultrasonic field $\cong 2.5^0$ was measured. This gives the value of the radiation force $F = P / v_{air} \cong 5.2 \cdot 10^{-6}$ H and the acoustic power $P \cong 1.8$ mW. Following the consideration of Section 2.1 we then obtain ≈ 5 mW/cm ^{2} of acoustic intensity and ≈ 200 Pa of pressure in the focus area.

Figure 3 demonstrates a 3D-frame of the wave field for the air-coupled flexural wave in 1.2 mm specimen of polycarbonate (commercial CD). The measured amplitude of vibration velocity in the centre of Fig. 3 is ≈ 250 μm/s (displacement $\approx 10^{-10}$ m) while the flexural wave amplitude is ~ 60 μm/s (displacement $\sim 2.5 \cdot 10^{-11}$ m). By using the experimental parameters of the focused beam determined above, the estimated amplitude of the displacement is $\approx 8 \cdot 10^{-11}$ m which is in a fair agreement with the measured data.

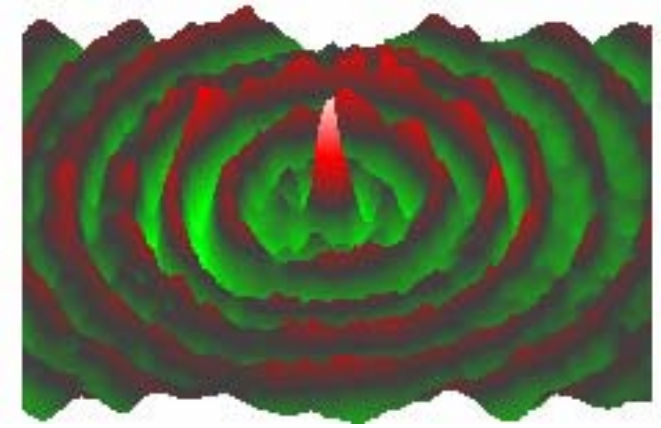

Figure 3. Wave field excited by focused air-coupled transducer in 1.2mm plate of polycarbonate.

Figure 4 (left) shows the wavefront pattern observed for the surface wave in a PMMA specimen (thickness 25 mm). The circular wavefronts clearly demonstrate the in-plane isotropy of the material. On the contrary, the wavefronts of flexural waves in a 2-mm unidirectional specimen of carbon fibre reinforced plastic (CFRP) (Figure 4 (right)) are ellipticalyl elongated along the fibre direction. The ratio of the ellipse axes in Figure 4 is ≈ 1.3 which agrees well with direct measurements of the phase velocity by FSTM [13] along and across the fibres in this specimen.

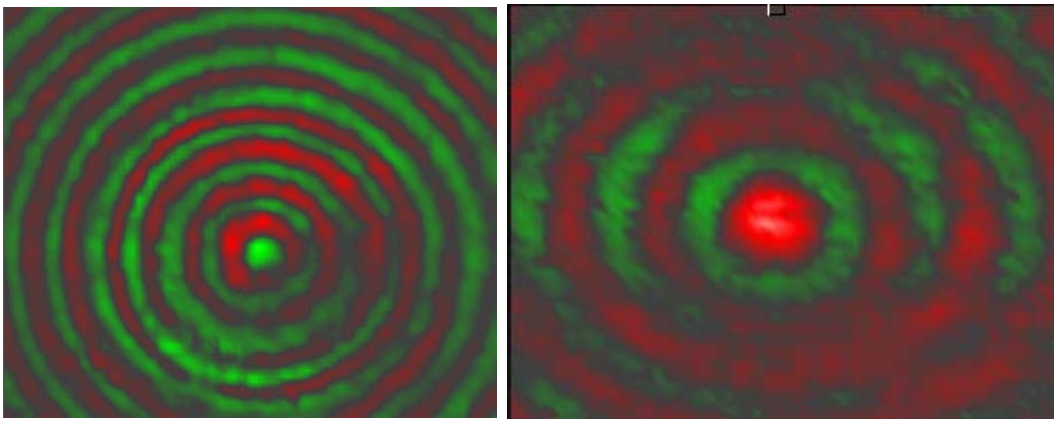

Figure 4. Wavefront patterns for SAW in PMMA (left) and flexural wave in CFRP (right).

Another example of application of the wavefront imaging for NDT of fibre orientation in composites is shown in Figure 5. The results are presented for a 2-mm thick

fibre-reinforced polyamide sample (30% (weight) of short glass fibres) manufactured by injection moulding. To simulate a controllable deviation in the fibre orientation, a rhomb-like barrier (black, Figure 5, a) was placed in the mould thereby bending the flow direction and generating a weldline. As a result, one would expect a vertical fibre direction in the middle of the plate (area B) and the fibre slopes of opposite signs around (A and C). This was confirmed by LSM-measurements of the surface distribution of the fibre directions (Figure 5, a). The wavefront images reveal the ellipse-shaped flexural wavefronts in the areas A–B-C (Figure 5, b). By comparing with the optical measurements, one can see that the orientation of the "fast" axis of the ellipse (slope of the ellipse) indicates a local fibre direction.

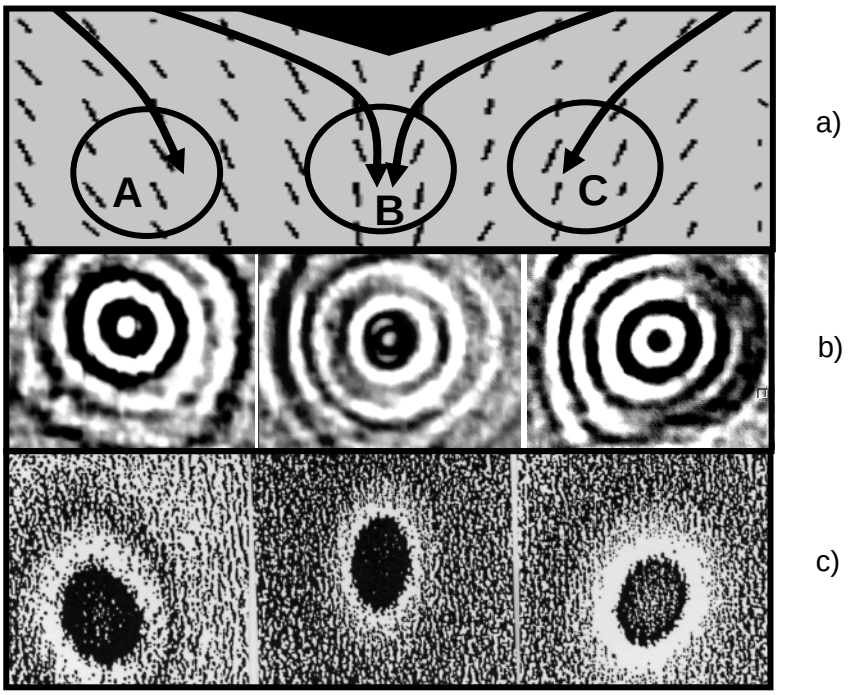

Figure 5. Measurements of local fibre anisotropy in short glass fibre reinforced composites.

Figure 5, c) shows the results of the thermal wave experiment reported for the same configuration in injection moulded CFRP [14]. The methodology makes use of the lock-in principle for a sensitive imaging of the thermal wavefronts excited by a point-like source of modulated heat. A striking similarity between the results in Figures 5 a) and b) confirms the fact that even low-frequency acoustic waves simulate closely heat transport by high-frequency phonons. It also shows that the elastic anisotropy governs the propagation not only of ballistic phonons [2] but also diffusive phonons at room temperature.

Acoustic wave propagation along the "fast" directions in composites can be accompanied by focusing of the energy flow. One of the reasons for that is concerned with "compacting" of the $\vec{v}_g$ vectors around the reinforcement direction which happens to be only for a particular anisotropy of the phase velocity [2]. Another factor characteristic for composites comes from a specific fibrous structure of these materials. Firstly, this results in anisotropy of dissipation: acoustic wave scattering rises dramatically in the direction normal to them. Secondly, a pair of rigid fibres with a soft matrix in between represents a typical waveguide in which the energy is focused in the slow section due to refraction of the wave field in the faster casing (analogous to a fibre-optic waveguide).

Such an effect is demonstrated in Figure 6 for the surface wave incident on a notch in a softwood (LT-plane) specimen. Wood is a natural composite with a fibrous structure of

a μm-scale. Another factor which contributes to the reinforcement of wood at meso- (mm-scale) is determined by seasonal variation of local stiffness due to the difference of fibre quality in annual rings. Each ring comprises a pair of fast fibre layers of latewood separated by a wider area of slow earlywood [15]. The waveguide effect is clearly seen in Figure 6: the wavefront of initially plane surface wave excited by the air-coupled transducer ($\theta \approx 20^0$ in the set-up of Figure 1) is parted and trapped inside the earlywood areas of the annual rings. The amplitude enhancement due to focusing inside the waveguide reaches ≈ 30 dB; the focusing recovers promptly even after diffuse scattering of the wave by the notch.

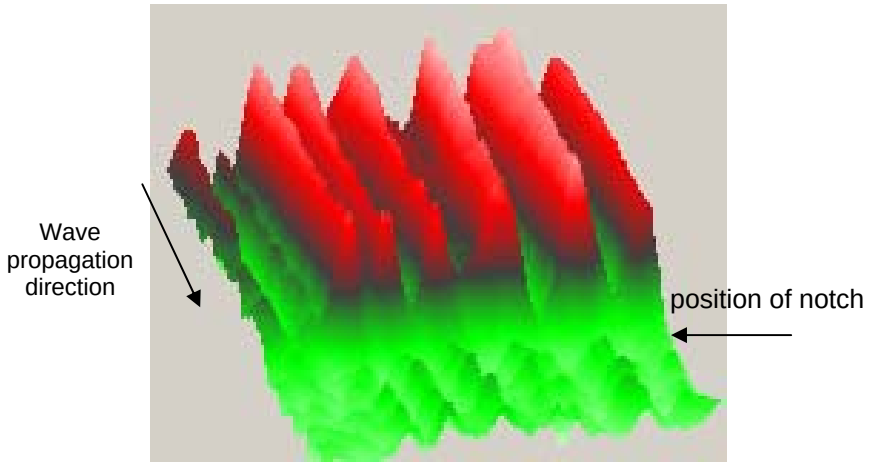

Figure 6. Fonon focusing due to waveguide effect in annual rings of wood.

All of the above mentioned factors possibly contribute to phonon focusing of omnidirectional acoustic waves in composites. This effect is illustrated in Figure 7 for a point-like air-coupled source exciting flexural waves in a single-component (liquid crystal fibres) composite. Besides the evident anisotropy indicated by the wavefront elongation along the fibres, a strong increase in scattering is observed as the wavefront deviates from the fast direction (Figure 7, left). As a result, the wavefield transforms into a weakly-diffracting acoustic beam with $\cong 10$ dB of the amplitude enhancement (Figure 7, right) which propagates at substantially longer distance along the fibres.

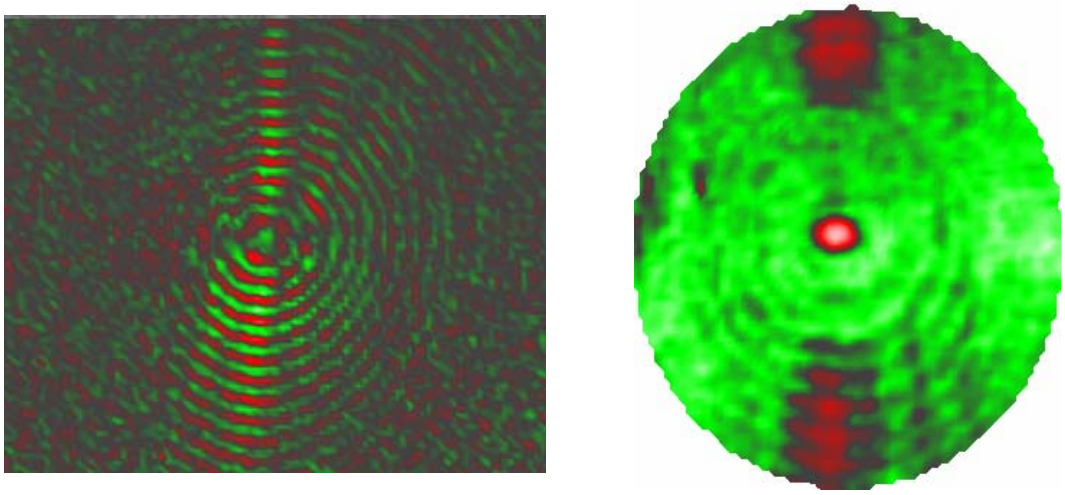

Figure 7. Phonon-focusing of air-coupled flexural wave in a single-component composite: view over the scanning area 35x30 mm (linear scale, left); zoomed image in dB-scale (right).

References

[1]. B.A. Auld, *Acoustic fields and wave in solids*, v. 1, John Wiley & Sons, New York, 1973.
[2]. J. P. Wolf, *Imaging phonons: acoustic wave propagation in solids*, Cambridge University press, Cambridge, 1998.
[3]. A.G. Every, W. Sachse, K.Y. Kim, and M.O. Thompson, Phonon focusing and mode-conversion effect in silicon at ultrasonic frequencies, Phys. Rev. Letts., v. 65, N. 12, pp. 1446-1449, 1990.
[4]. Y. Sugawara, O.B. Wright, O. Matsuda, M. Takigahira, Y. Tanaka, S. Tamura, and V. Gusev, Phys. Rev. Letts., v. 88, 185504, 2002.
[5]. A.A. Maznev, Al.A. Kolomenskii, and P. Hess, Time-Resolved cuspidal structure in the wave front of surface acoustic pulses on (111) galium arsenide, Phys. Rev. Letts., v. 75, N 18,pp. 3332-3335, 1995.
[6]. Al.A. Kolomenskii and A.A. Maznev, Phonon-focusing effect with laser-generated ultrasonic surface waves, Phys. Rev. B, v. 48, N 19, pp. 502-508, 1993.
[7]. M. Veidt and W. Sachse, Ultrasonic point-source/point-receiver measurements in thin specimens, J. Acoust. Soc. Am., v. 96, N 4, pp. 2318-2326, pp. 1994.
[8]. M.R. Hauser, R.L. Weaver, and J.P. Wolf, Internal diffraction of ultrasound in crystals: phonon focusing at long wavelengths, Phys. Rev. Letts., v. 68, 2604, 1992.
[9]. I. Solodov, K. Pfleiderer, and G. Busse, Laser vibrometry of air-coupled Lamb waves: a novel methodology for non-contact material characterization, Materialprüfung, 47, 3, pp. 3-7, 2005.
[10]. I.A. Victorov. *Rayleigh and Lamb Waves*, Plenum Press, N[ew York (1967).
[11]. G. Kino, *Acoustic waves: devices, imaging, and analog signal processing*, Prentice-Hall Inc., Englewood Cliffs, New Jersey , 1987.
[12]. G.A. Korn and T.M. Korn, *Mathematical Handbook*, McGraw-Hill, 1968.
[13]. I. Yu. Solodov, R. Stoessel, G. Busse, Material characterization and NDE using focused slanted transmission mode of air-coupled ultrasound, Research in Non-Destructive Evaluation, v.15, pp. 1-21, 2004.
[14]. W. Karpen, D. Wu, R. Steegmüller, and G. Busse, Depth profiling of orientation in laminates with local lock-in thermography, Proc. QIRT`94, Sorrento, Italy, pp. 281-286, 1994.
[15]. Igor Solodov, Klaus Pfleiderer and Gerhard Busse, Nondestructive characterization of wood by monitoring of local elastic anisotropy and dynamic nonlinearity, Holzforschung, v. 58, pp. 504-510, 2004.